Report

Transcriptome stability profiling identifies novel and functional MIRNA targets in melanoma cells

Piyush Joshi[1, 2, 3], Tatsuya Seki[3, 4], Andrea Bergano[3], John Marchica[2, 3], Shinobu Kitamura[4] and Ranjan J. Perera* [2, 3,5]

[1] Department of Oncology, Johns Hopkins University School of Medicine, 401 N. Broadway, Baltimore, MD 21287 USA

[2] Department of Cancer and Blood Disorders Institute, Johns Hopkins All Children's Hospital, 600 5th St. South, St. Petersburg, FL 33701 USA

[3] Sanford Burnham Prebys Medical Discovery Institute, 6400 Sanger road, Orlando, FL 32827 USA

[4] Medical and Biological Laboratories, Nagoya 460-0008, Japan

[5] The Sidney Kimmel Comprehensive Cancer Center, Johns Hopkins University School of Medicine, 401 N. Broadway, Baltimore, MD 21287 USA

*Corresponding author email: jperera2@jhmi.edu

Running head: Transcriptome stability profiling in melanoma

Keywords: BRIC-seq; RNA-seq; melanoma; MIRNA; RNA stability

ABSTRACT (181 words)

Melanoma has a high propensity to metastasize and is often lethal. Effective biomarkers and therapies are lacking, so candidate identification remains a clinical priority. RNA half-life is closely related to its cellular physiological function, and stability determinants may therefore have regulatory functions. Micro(MI)RNAs have primarily been studied with respect to post-transcriptional mRNA regulation and target degradation. Here we study the impact of tumor suppressive melanoma MIRNA MIR211 on transcriptome stability and phenotype in the A375 amelanotic melanoma cell line. Using 5'-bromouridine IP chase (BRIC)-seq, transcriptome-wide RNA stability profiles revealed highly regulated genes and pathways important in this melanoma cell line. Using a combinatorial approach of BRIC-seq, RNA-seq, and *in silico* predictions, we identify both existing and novel direct MIR211 targets. *DUSP3* is validated as one such novel MIR211 target, which itself sustains colony formation and invasion in A375 cells, probably via MAPK/PI3K signaling. MIRNAs have the capacity to control RNA turnover as a gene expression mechanism. RNA stability profiling is an excellent tool for interrogating functionally relevant cancer pathways and MIRNA targets when combined with other high-throughput and *in silico* approaches.

INTRODUCTION

Melanoma is the commonest cause of skin cancer-related deaths, with an estimated 90,000 diagnoses and 10,000 deaths in the US in 2018 (Siegel et al. 2018). The high mortality associated with melanoma is due to its intrinsic aggressiveness, metastatic potential, and resistance to conventional therapies (Pawlik and Sondak 2003). There is a pressing need to better understand the abnormal biological processes contributing to melanoma development, metastasis, and resistance to develop new biomarkers and therapies.

Whole transcriptome sequencing (RNA-seq) is now a standard method to interpret the cellular state during disease development and progression. However, RNA-seq represents a static image of the process of transcription, while biological processes are by their very nature dynamic. Recent studies on transcriptome dynamics have shown that transcript stability is correlated with function (Yang et al. 2003; Narsai et al. 2007; Lugowski et al. 2018; Mitra et al. 2018). For instance, transcription factor mRNAs have high average decay rates (Yang et al. 2003), and mRNA turnover correlates with signaling pathways active in cancer, suggesting a post-transcriptional component to oncogenesis (Benjamin and Moroni 2007). Hence, understanding transcript dynamics is important for understanding disease pathogenesis including in cancer.

mRNA decay studies have traditionally been dominated by the use of transcriptional inhibitors such as actinomycin D (Singer and Penman 1972; Mitra et al. 2018) or α-amanitin (Alkallas et al. 2017; Lugowski et al. 2018) to arrest transcription. mRNA concentrations are then quantified at progressive time points after transcriptional arrest. However, these transcriptional inhibitors stress cells and themselves alter transcript localization, stability, and cellular proliferation, introducing unintended and confounding variables (Bensaude 2011; Tani et al. 2012). More recent metabolic nucleotide labeling techniques such as with 5-bromouridine (Tani et al. 2012; Imamachi et al. 2014), 4-thiouridine (Tani et al.

2012; Lugowski et al. 2018), or 5-ethynyluridine (Diermeier-Daucher et al. 2009) have overcome these limitations by providing a direct read-out of transcript decay. Here we exploit the recently described 5'-bromouridine IP chase (BRIC)-seq assay (Tani et al. 2012; Imamachi et al. 2014), in which the nucleotides of newly synthesized transcripts are labeled with 5-bromouridine (BrU), to study transcriptomic stability in melanoma cells. Coupling BrU labeling with RNA-seq quantifies global RNA (mRNAs and long non-coding (lncRNAs)) stability over time without unduly perturbing the environment (Tani et al. 2012; Imamachi et al. 2014; Imamachi et al. 2017).

MicroRNAs (MIRNAs) are a class of single-stranded short noncoding RNA, typically 22 nucleotides long in the mature form (Ha and Kim 2014). MIRNAs are well known post-transcriptional regulators in both health and disease (Peng and Croce 2016; Alberti and Cochella 2017). MIRNAs tend to repress gene expression by binding to MIRNA-specific sites in the 3' UTR of the target mRNA in conjugation with the AGO protein-containing RNA-induced silencing complex (RISC) (Kawamata and Tomari 2010). Altered regulation of MIRNAs or their targets is common in cancers, with MIRNA dysregulation shown to have both oncogenic and tumor suppressive roles (Hayes et al. 2014; Peng and Croce 2016). Further, MIRNA targets tend to have shorter half-lives (Narsai et al. 2007), so MIRNA have a direct impact on steady-state transcript levels and ultimately protein activity. Thus, a MIRNA-induced change in transcript stability, for example of oncogenes or tumor suppressor genes, has functional consequences (Benjamin and Moroni 2007; Khabar 2017).

Here we explore the transcriptome stability of the stage IV amelanotic melanoma cell line A375 to better understand its role in melanoma development and progression. We also investigate RNA dynamics in the presence and absence of MIR211, which acts as a tumor suppressor in this cell line (Mazar et al. 2010; Mazar et al. 2016). We show that MIR211 decreases transcriptome stability. MIR211-dependent destabilization also downregulates several target genes and pathways involved in cancer progression. Using a combination of stability dynamics, gene expression changes, and *in silico* prediction; we decipher

transcriptome-wide MIR211 targets in A375 cells. Focusing on one such target gene, *DUSP3*, we show that its MIR211-dependent downregulation modulates signaling pathways and the cancer phenotype *in vitro*. Overall, the study provides insights into the dynamic interplay between MIR211 and its targets and how these interactions contribute to melanoma genesis.

RESULTS AND DISCUSSION

Transcriptomic stability and decay in the A375 amelanotic melanoma cell line

We were motivated to study the transcriptome stability of A375 amelanotic melanoma cells to better understand the relationship between mRNA stability and tumor phenotype. To this end, we used BRIC-seq to quantify transcriptome-wide stability (Imamachi et al. 2014; Imamachi et al. 2017). A375 cells were subjected to BRIC-seq at four timepoints (0, 1, 3, and 6 h) (**Fig. 1A**) to determine transcript decay rate or half-life. BrU labelled RNA was pulled down using an anti-BrdU antibody before being deep sequenced and processed to obtain read counts normalized to spike-in control RNA (see Methods). Normalized RNA reads were filtered for quality to obtain the decay profile (**Fig. 1B**), which was converted into half-lives (**Fig. 1C, Table S1**).

At the transcriptome-wide level, the majority of transcripts decayed over time (**Fig. 1B**). Overall, transcripts had half-lives of under 2 h (mean 1.459 h, median 1.248 h) (**Fig. 1C**), with mRNA stability (mean 1.512 h, median 1.324 h) higher than lncRNA stability (mean 1.077 h, median 0.9364 h) but comparable to pseudogene stability (mean 1.564 h, median 1.248 h) (**Fig. 1C**). BRIC-seq quantified half-lives were validated by BRIC-qPCR for selected candidates, and *MYC* and GAPDH half-lives were within 20% of the deep sequencing estimate and half-life ratios were comparable (**Fig. S1**).

We next established whether transcript stability was associated with gene function in A375 cells. Gene ontology (GO) analysis showed that the top 5% most stable coding transcripts had a housekeeping

function (e.g., mitochondrial function, metabolic processes, and enzyme binding), while the top 5% most unstable coding transcripts tended to be important for transcription regulation (e.g., nucleic acid binding transcription factor activity, double-stranded DNA binding, negative regulation of gene expression; **Fig. 1D**), similar to observed in other genome-wide decay studies using different methodologies (Yang et al. 2003; Narsai et al. 2007; Clark et al. 2012; Tani et al. 2012). With respect to "hallmark" signatures (Subramanian et al. 2005), the most stable transcripts were enriched for genes involved in epithelial to mesenchymal transition and MYC signaling in addition to housekeeping metabolic pathways such as oxidative phosphorylation (**Fig. 1E**), while unstable transcripts were enriched for signaling pathways that play significant role in melanoma progression such as TNFα (Katerinaki et al. 2003; Gray-Schopfer et al. 2007), p53 (Box et al. 2014), and TGTβ (Busse and Keilholz 2011; Perrot et al. 2013). Interestingly, unstable genes were enriched for genes downregulated by UV radiation (Giles et al. 2012) and KRAS signaling (Ji et al. 2012; Frederick et al. 2013), two common drivers of melanoma progression. Overall, many pathways and processes are regulated at the RNA stability level, with the unstable decay profiles identifying highly regulated genes and pathways important in melanoma progression.

MIR211-mediated decay targets coding and non-coding transcripts

To better understand the role of MIRNAs in transcript stability and cancer progression in A375 cells, we next determined transcriptome stability dynamics in A375 cells overexpressing MIR211 (A375/211 cells), a known tumor suppressor (**Fig. 2A, Fig. 2B**) (Mazar et al. 2010; Xu et al. 2012; Mazar et al. 2016). MIR211 overexpression reduced the half-lives of all RNA species, especially mRNAs (mean 1.297 h, median 1.170 h, 14% reduction compared to parental cells) and pseudogenes (mean 1.365 h, median 1.187 h, ~13% reduction compared to parental cells; **Fig. 2C**). While MIR211 overexpression had little effect on the half-life distribution (**Fig. 2C**), the highest stability changes occurred in the most stable A735 transcripts (**Fig. 2D**), accounting for the lower mean half-lives for each transcript species.

GO and hallmark analysis suggested that MIR211 preferentially decreased the half-lives of genes involved in metabolic and energy-generating activities (**Fig. 2E**, **Fig. 2F**), some of which such as oxidative phosphorylation/energy metabolism (Mazar et al. 2016; Sahoo et al. 2017; Guda et al. 2018; Sahoo et al. 2019), lipid/fatty acid metabolism (Barbato et al. 2017; Sahoo et al. 2017), mitosis/cell-cycle progression/cell-cycle checkpoint (Asuthkar et al. 2012; Song and Zhao 2015; Xia et al. 2015), and MYC-dependent signaling (Chu et al. 2013; Bu et al. 2018) have already shown to be regulated by MIR211 in cancer and other diseases. This altered regulation extended to the individual pathway level, with gene set enrichment analysis (GSEA) for Biocarta pathways showing that integrin signaling, involved in cell shape and mobility, was enriched in destabilized protein-coding transcripts (data not shown), in line with our previous observation of drastically altered shape of A375/211 cells compared to A375 cells (Mazar et al. 2016). Taken together, these results suggest that MIR211 drives transcript stability changes in A375 cells that are associated with functional outcomes.

MIR211 target prediction using BRIC-seq stability data

MIR211 might destabilize transcripts through both direct (MIR211 binding to the 3'UTR of the target mRNA with the RISC complex to degrade mature transcript) or indirect (destabilized through overall changes in the regulatory state of the cell) regulation. The observed level of an individual transcript will be governed by both the degradation rate and the transcription rate.

Given that MIRNAs directly degrade transcript, we reasoned that direct MIR211 targets will have (i) lower stability (i.e., decreased half-lives, =< 80%) in A375/211 cells than in parental A375 cells; (ii) lower expression levels (**Fig. 3A**), and (iii) MIR211 target sequences in their 3'UTRs. Using this stringent approach, 16 protein-coding genes (**Fig. 3B** and **Fig. 3C**) had a high probability of being MIR211 targets, and indeed *PDK4* and *EFEMP2* have been shown to be direct MIR211 targets in melanoma (Bell et al. 2014; Mazar et al. 2016). GO analysis of the selected candidates suggested that MIR211 directly targets genes related to cellular metabolism, and several of the predicted MIR211 targets have been implicated in

the development and progression of other cancers; for example, *ANO5* is downregulated in thyroid cancer (Chang et al. 2017); *GREB1* is upregulated in ovarian (Hodgkinson et al. 2018), breast (Ghosh et al. 2000), and prostate cancers (Rae et al. 2006); and *EFEMP2* is upregulated in glioma (Wang et al. 2015) and colorectal cancers (Yao et al. 2012). Some previously predicted MIR211 targets in melanoma cell lines such as *RAB22A*, *SERINC3*, *AP1S2* (Margue et al. 2013); *NUAK1* (Bell et al. 2014); *BRN2/POU3F2* (Boyle et al. 2011) did not meet the criteria, suggesting that the approach shows some cell type specificity. Nevertheless, combining stability data with gene expression data and existing information appears to provide a highly stringent approach for identifying MIRNA targets.

DUSP3 is a MIR211 target in A375 where it promotes cancer progression

To examine whether our approach had successfully identified a hitherto unknown MIR211 target in melanoma, we selected *DUSP3* for further validation. *DUSP3*, also known as vaccinia-H1 related (VHR) (Ishibashi et al. 1992), has been shown to be functionally involved various cancers including cervical carcinoma (Henkens et al. 2008), prostate cancer (Arnoldussen et al. 2008), and breast cancer (Hao and ElShamy 2007). However, there are no reports of *DUSP3* involvement in melanoma or its regulation by MIR211.

We first validated DUSP3 as an MIR211 target. BRIC-qPCR ($t_{1/2}$; A375= 0.956 h, A375/211=0.775 h) (**Fig. 3E**) and RT-qPCR (**Fig. 3F**) showed that MIR211 upregulated the *DUSP3* transcript decay rate and downregulated *DUSP3* expression. There were two *in silico*-predicted MIR211-binding sites in the *DUSP3* 3'UTR (**Fig. 3G**), so we tested both sites for MIR211 targeting by transfecting cells with a luciferase vector containing native *DUSP3* 3'UTR or mutated (mut) *DUSP3* 3'UTR (**Fig. 3G**). The mutated 3'UTR abrogated MIR211-dependent downregulation of luciferase activity (**Fig. 3H**) compared to the native 3'UTR.

To understand whether MIR211-mediated *DUSP3* downregulation in melanoma was functional, we next performed loss-of-function experiments with siRNA knock-down of endogenous *DUSP3* in A375 cells (**Fig. 4A**). While MIR211 overexpression significantly reduced proliferation compared to parental A375 cells (**Fig. 4B**), siRNA knockdown of *DUSP3* in A375 cells did not affect proliferation (**Fig. 4B**). However, *DUSP3* knockdown reduced invasion and colony formation at comparable levels to those observed in A375/211 cells compared to A375 (**Fig. 4C, Fig. 4D**), suggesting that DUSP3 downregulation might contribute to MIR211-dependent regulation of cell invasion and anchorage-independent growth. DUSP3 has previously been shown to induce cell growth and inhibit apoptosis in adenocarcinoma cells (Arnoldussen et al. 2008), and *DUSP3* depletion in HeLa cells induces cell cycle arrest and reduces cell proliferation (Rahmouni et al. 2006). Furthermore, *DUSP3* knockout reduces cell migration (Chen et al. 2017) and inhibits *in vitro* angiogenic sprouting (Amand et al. 2014), consistent with the oncogenic function seen here.

DUSP3 is a dual activity phosphatase that regulates signaling pathways by dephosphorylating target tyrosine and/or serine/threonine residues (Huang and Tan 2012). While DUSP3 has been shown to specifically target ERK1/2 and JNK MAP kinase (MAPK) pathways (Rahmouni et al. 2006; Hao and ElShamy 2007; Amand et al. 2014; Tambe et al. 2016) in multiple cancers, its role in melanoma is unknown. To investigate the specific kinase pathway(s) regulated by DUSP3 in A375, we assessed phosphorylation of various MAPK pathway members using a MAPK array upon *DUSP3* knockdown (**Fig. 4E**). DUSP3 knockdown increased phosphorylation of pAKT, pERK1, pHSP27, p70 S6kinase, and pmTOR, similar to the pattern seen in A375/211 cells (**Fig. 4F**). While previous reports have suggested DUSP3 targets the ERK pathway, our observation suggests that DUSP3 also regulates PI3K/AKT signaling, not only upstream at the level of pAKT but also the downstream pathways members p70 S6kinase and pmTOR (**Fig. 4G**) (Hemmings and Restuccia 2012). Recent reports have suggested that HSP27 is associated with both the ERK and AKT pathways, suggesting the observed change in phosphorylation could be via these pathways (Rane et al. 2003; Robitaille et al. 2010; Deng et al. 2016).

Similar positive regulation of ERK (Hu et al. 2016) or AKT (Sahoo et al. 2019) by MIR211 has previously been reported in other cell lines. Taken together, these results support that MIR211 may exert some of its tumor suppressive function via downregulation of DUSP3 and related downstream pathways to inhibit growth and invasion.

CONCLUSIONS

Here we show that transcript stability is an important contributor to the cancer phenotype and that miRNAs have a global impact on transcript stability that might affect the cancer phenotype. We exploited a genome-wide transcript stability assay to identify context-dependent transcriptome-wide miRNA targets. Our combinatorial approach of using stability, differential expression, and *in silico* prediction proved to be a stringent method to identify functionally relevant and novel MIRNA targets. We show that the novel direct MIR211 target DUSP3 has an oncogenic role in A375 melanoma cells. Finally, our results support the role of MIR211-dependent regulation of DUSP3 in regulating melanoma growth and progression by modulating MAPK/PI3K signaling.

Materials and methods

Cell culture

The human stage IV amelanotic melanoma cell line A375 (ATCC Number: CRL-1619) and the derived MIR211 overexpressing A375/211 cell line (Mazar et al. 2010) were grown in Tu+ medium as previously described (Mazar et al. 2010).

BRIC-Seq and BRIC-qPCR

A375 and A375/211 cells were incubated with metabolic bromouridine (BrU) for 24 h and then used as per the BRIC kit (RN1007/1008; MBL International, Woburn, MA) protocol. Briefly, labeled medium was replaced with fresh medium and cells were collected at 0, 1, 3, and 6 h post labeling. Total RNA was

extracted using the Direct-zol RNA miniprep kit (R2060, Zymo Research, Irvine, CA) mixed with external spike-in labeled RNA according to the manufacturer's recommendation before pulling down labeled RNA with an anti-BrdU antibody (BRIC kit). Bound RNA was eluted and followed by RT-qPCR or deep sequencing.

RNA extraction, cDNA synthesis, and qPCR

Total RNA was isolated from cells using the Direct-zol RNA miniprep kit (R2060, Zymoresearch), with subsequent quantification using Nanodrop (Thermofisher). TaqMan probes were used to quantify *DUSP3* (Hs01115776_m1) using *GAPD* (Hs99999905_m1) and *ACTB* (Hs1060665_g1) as control. Standard qPCR primers were used for *GAPDH*, *MYC* and BRIC-spike in control for BRIC-qPCR. Fold change was obtained from Ct value comparison. Fold change from different condition was compared using two-tailed Student's t-test assuming equal variance.

RNA-seq

RNA sequencing was done at the Genomics Core at the Sanford Burnham Prebys, Orlando, FL. Before sequencing, total RNA quality was assessed with the Agilent Bioanalyzer Nano Assay (Part no. 5067-1512) (Agilent Technologies). RNA-seq libraries were constructed using the Illumina TruSeq Stranded Total RNA Library preparation Gold kit (catalog no. 20020598) (Illumina Inc., San Diego, CA) as per the instructions. The quality and quantity of the libraries were analyzed using the Agilent Bioanalyzer and Kapa Biosystems qPCR (Sigma-Aldrich). Multiplexed libraries were pooled, and single-end 50 base-pair sequencing was performed on one flow-cell of an Illumina HiSeq 2500.The RNA-seq data has been uploaded on GEO, accession number (awaiting accession number).

The reads were mapped to GRCh38/hg38 human genome assembly p12 (release 28, www.gencodegenes.org) using HISAT2 and annotated using corresponding release version gencode

comprehensive annotation file. Mapped reads were quantified using StringTie to obtain FPKM values, which were converted to read counts using prepDE.py script (provided in StringTie manual).
For differential gene expression analysis reads count from two independent samples for A375 and A375/211 each were analyzed by DESeq2 script in R (Love et al. 2014).

Decay rate analysis

For BRIC-seq decay analysis, read counts from 4 time points (0, 1, 3 and 6 h) were normalized to that of spike-in RNA counts to obtain normalized read counts. Normalized read counts at time 1/3/6 h were scaled with respect to 0 h reads. The decay constant was obtained from normalized and scaled read counts by fitting it to a linear model (log(y)=x+c) using R (www.R-project.org). Data with positive decay constant or R-squared values <0.75 in both A375 and A375/211 conditions were removed from further analysis. Decay constant was converted into half-life from relation $t_{1/2}=-0.693/decay_constant$.
For BRIC-qPCR decay analysis, fold change of genes were obtained with respect spike-in RNA at each time point. Fold change at time points 1/3/6 h were then scaled to that at 0 h and fitted on to a exponential curve to obtain decay constant that was converted to half-life as described above.

GSEA and Gene Ontology (GO) analysis

Genes selected for GO term and hallmark analysis were subjected to functional annotation on GSEA web-based application (broad.mit.edu/gsea/) (Subramanian et al. 2005). GSEA enrichment analysis for decay ratio was conducted with GSEAPreranked list with rank determined by decay rate ratio between A375 vs A375/211.

Target cleavage assays

The 3′ UTR sequences of *DUSP3* (NM004090) mRNA genes were amplified by PCR using the primers (forward: AGTGGCAGGGCGGCCGCCACTGCCGGGAAGGTTATAGC, reverse:

GGTGATGATGACCGGTAGCGAGTCCAATTGCTTCATGTG) using A375 genomic DNA. The forward and reverse primer contained 5′ NotI or 3′ AgeI (underscored sequence), respectively. The PCR product was cloned into pcDNA6/luc/NP3 into a NotI-AgeI site using the Clontech In-Fusion kit (Clontech Laboratories, Mountain View, CA). To remove the two putative MIR211 sites, mutated *DUSP3* 3'UTR was engineering via site-directed mutagenesis using the primers: first site (XhoI site) CACCAACATTCTCGAGCCAAACCATCCATCACCATG, reverse: GATGGTTTGGCTCGAGAATGTTGGTGCCTTTTGTGCC; second site (AvrII site), forward: TGGTAGCTCTCCTAGGTCTGTCCAGAAAAATTCACTC, reverse: TCTGGACAGACCTAGGAGAGCTACCAAATTGTTT. The mutated insert was cloned into the same insertion site of a luciferase vector. HEK293T cells were transfected with *DUSP3* 3'UTR or mutated 3'UTR(*DUSP3mut*) with and without MIR211 overexpression construct (as described in (Sahoo et al. 2019)). After 48 h incubation, cells were washed in PBS and lysed using cell lysis buffer (Promega, Madison, WI). The lysate was quantified for firefly and renilla luciferase activity using Dual-Glo Luciferase assay system (Promega) to determine MIR211-dependent target instability.

DUSP3 siRNA knockout

A375 cells were transfected with siRNA against DUSP3 (siDUSP3) mRNA (s4371, Ambion) to achieve downregulation of DUSP3 expression. Negative control siRNA (siNEG) (AM4635, Ambion) was used as a control for the assay.

Cell proliferation assay

Cells were plated in triplicate at 5000 cells per well into 96-well plates for the various time points indicated in the figures and legends. Cell proliferation was assessed using the CellTiter96 Aqueous One Solution Cell Proliferation Assay (MTS) kit (Promega, Madison, WI).

Cell invasion assay

Cell invasion assay was performed using Corning BioCoat Matrigel Invasion Chambers (Discovery Labware, Bedford, MA) according to the manufacturer's protocol. Briefly, cells were starved in FBS-free medium for 24 h before being transferred into the upper chambers in serum-free medium (50,000 cells per chamber). Medium containing 10% FBS was added to the lower chambers. Cells were incubated for 48 h at 37ºC. To quantify cell invasion, migrated cells were stained with 0.5% crystal violet dye. Excess staining was removed by rinsing with water and subsequently membrane was dried before taking images. Dye from stained cells was extracted using methanol, and optical density was measured at 570 nm on a spectrophotometer to quantify cell invasion intensity.

Western blotting and MAPK phosphoarray

Whole cell extracts from A375 cell, A375 cells transfected with siNEG or siDUSP3 and A375/211 cells were fractionated by SDS-PAGE and transferred to a polyvinylidene difluoride membrane using a transfer apparatus according to the manufacturer's protocols (Bio-Rad). After incubation with blocking buffer containing 5% BSA in TBST (10 mM Tris, pH 8.0, 150 mM NaCl, 0.5% Tween 20) for 60 min, the membrane was washed once with TBST and incubated with antibodies against DUSP3 (4752, Cell Signaling), and β-Actin (4967, Cell Signaling) diluted in blocking buffer at 4 °C for 16 h. Membranes were washed three times for 10 min and incubated with a 1:3000 dilution of horseradish peroxidase-conjugated anti-mouse or anti-rabbit antibodies for 2 h. Blots were washed with TBST three times and developed with the ECL system (Amersham Biosciences) according to the manufacturer's protocols.
To determine the phosphorylation level of various MAPK pathway members, the phospho-MAPK array assay was done using Human phospho-MAPK array kit (R&D systems) according to the provided protocol.

AUTHOR CONTRIBUTIONS

PJ and TS performed and analyzed BRIC-seq experiment

PJ and AB performed and analyzed IHC experiments

JM prepared RNA-seq libraries and performed sequencing

BL constructed *DUSP3* and *DUSP3mut* constructs

PJ performed and analyzed rest of the experiments

PJ and RJP wrote the manuscript

CONFLICT OF INTEREST

RJP has been granted patent "miR-211 expression and related pathways in human melanoma" (#9994915).

FUNDING

This work was supported by National Institutes of Health grants [R21CA202197, CA165184, NCI 5P30CA030199 (SBP), P30 CA006973 (JHU SKCCC)] and Florida Department of Health, Bankhead-Coley Cancer Research Program [5BC08] to R.J.P.

ACKNOWLEDGEMENTS

We thank Sanford Burnham Prebys Medical Discovery Institute Analytical Genomics core for their support with RNA sequencing. Part of this research project analysis was conducted using computational resources at the Maryland Advanced Research Computing Center (MARCC).

REFERENCES

Alberti C, Cochella L. 2017. A framework for understanding the roles of miRNAs in animal development. *Development (Cambridge, England)* **144**: 2548-2559.

Alkallas R, Fish L, Goodarzi H, Najafabadi HS. 2017. Inference of RNA decay rate from transcriptional profiling highlights the regulatory programs of Alzheimer's disease. *Nature communications* **8**: 909.

Amand M, Erpicum C, Bajou K, Cerignoli F, Blacher S, Martin M, Dequiedt F, Drion P, Singh P, Zurashvili T et al. 2014. DUSP3/VHR is a pro-angiogenic atypical dual-specificity phosphatase. *Molecular cancer* **13**: 108.

Arnoldussen YJ, Lorenzo PI, Pretorius ME, Waehre H, Risberg B, Maelandsmo GM, Danielsen HE, Saatcioglu F. 2008. The mitogen-activated protein kinase phosphatase vaccinia H1-related protein inhibits apoptosis in prostate cancer cells and is overexpressed in prostate cancer. *Cancer research* **68**: 9255-9264.

Asuthkar S, Velpula KK, Chetty C, Gorantla B, Rao JS. 2012. Epigenetic regulation of miRNA-211 by MMP-9 governs glioma cell apoptosis, chemosensitivity and radiosensitivity. *Oncotarget* **3**: 1439-1454.

Barbato S, Marrocco E, Intartaglia D, Pizzo M, Asteriti S, Naso F, Falanga D, Bhat RS, Meola N, Carissimo A et al. 2017. MiR-211 is essential for adult cone photoreceptor maintenance and visual function. *Sci Rep* **7**: 17004.

Bell RE, Khaled M, Netanely D, Schubert S, Golan T, Buxbaum A, Janas MM, Postolsky B, Goldberg MS, Shamir R et al. 2014. Transcription factor/microRNA axis blocks melanoma invasion program by miR-211 targeting NUAK1. *The Journal of investigative dermatology* **134**: 441-451.

Benjamin D, Moroni C. 2007. mRNA stability and cancer: an emerging link? *Expert opinion on biological therapy* **7**: 1515-1529.

Bensaude O. 2011. Inhibiting eukaryotic transcription: Which compound to choose? How to evaluate its activity? *Transcription* **2**: 103-108.

Box NF, Vukmer TO, Terzian T. 2014. Targeting p53 in melanoma. *Pigment cell & melanoma research* **27**: 8-10.

Boyle GM, Woods SL, Bonazzi VF, Stark MS, Hacker E, Aoude LG, Dutton-Regester K, Cook AL, Sturm RA, Hayward NK. 2011. Melanoma cell invasiveness is regulated by miR-211 suppression of the BRN2 transcription factor. *Pigment cell & melanoma research* **24**: 525-537.

Bu Y, Yoshida A, Chitnis N, Altman BJ, Tameire F, Oran A, Gennaro V, Armeson KE, McMahon SB, Wertheim GB et al. 2018. A PERK-miR-211 axis suppresses circadian regulators and protein synthesis to promote cancer cell survival. *Nature cell biology* **20**: 104-115.

Busse A, Keilholz U. 2011. Role of TGF-beta in melanoma. *Current pharmaceutical biotechnology* **12**: 2165-2175.

Chang Z, Cai C, Han D, Gao Y, Li Q, Feng L, Zhang W, Zheng J, Jin J, Zhang H et al. 2017. Anoctamin5 regulates cell migration and invasion in thyroid cancer. *International journal of oncology* **51**: 1311-1319.

Chen YR, Chou HC, Yang CH, Chen HY, Liu YW, Lin TY, Yeh CL, Chao WT, Tsou HH, Chuang HC et al. 2017. Deficiency in VHR/DUSP3, a suppressor of focal adhesion kinase, reveals its role in regulating cell adhesion and migration. *Oncogene* **36**: 6509-6517.

Chu TH, Yang CC, Liu CJ, Lui MT, Lin SC, Chang KW. 2013. miR-211 promotes the progression of head and neck carcinomas by targeting TGFbetaRII. *Cancer Lett* **337**: 115-124.

Clark MB, Johnston RL, Inostroza-Ponta M, Fox AH, Fortini E, Moscato P, Dinger ME, Mattick JS. 2012. Genome-wide analysis of long noncoding RNA stability. *Genome research* **22**: 885-898.

Deng W, Zhang Y, Gu L, Cui J, Duan B, Wang Y, Du J. 2016. Heat shock protein 27 downstream of P38-PI3K/Akt signaling antagonizes melatonin-induced apoptosis of SGC-7901 gastric cancer cells. *Cancer cell international* **16**: 5.

Diermeier-Daucher S, Clarke ST, Hill D, Vollmann-Zwerenz A, Bradford JA, Brockhoff G. 2009. Cell type specific applicability of 5-ethynyl-2'-deoxyuridine (EdU) for dynamic proliferation assessment in flow cytometry. *Cytometry Part A : the journal of the International Society for Analytical Cytology* **75**: 535-546.

Frederick DT, Piris A, Cogdill AP, Cooper ZA, Lezcano C, Ferrone CR, Mitra D, Boni A, Newton LP, Liu C et al. 2013. BRAF inhibition is associated with enhanced melanoma antigen expression and a more favorable tumor microenvironment in patients with metastatic melanoma. *Clinical cancer research : an official journal of the American Association for Cancer Research* **19**: 1225-1231.

Ghosh MG, Thompson DA, Weigel RJ. 2000. PDZK1 and GREB1 are estrogen-regulated genes expressed in hormone-responsive breast cancer. *Cancer research* **60**: 6367-6375.

Giles N, Pavey S, Pinder A, Gabrielli B. 2012. Multiple melanoma susceptibility factors function in an ultraviolet radiation response pathway in skin. *The British journal of dermatology* **166**: 362-371.

Gray-Schopfer VC, Karasarides M, Hayward R, Marais R. 2007. Tumor necrosis factor-alpha blocks apoptosis in melanoma cells when BRAF signaling is inhibited. *Cancer research* **67**: 122-129.

Guda MR, Asuthkar S, Labak CM, Tsung AJ, Alexandrov I, Mackenzie MJ, Prasad DV, Velpula KK. 2018. Targeting PDK4 inhibits breast cancer metabolism. *Am J Cancer Res* **8**: 1725-1738.

Ha M, Kim VN. 2014. Regulation of microRNA biogenesis. *Nature reviews Molecular cell biology* **15**: 509-524.

Hao L, ElShamy WM. 2007. BRCA1-IRIS activates cyclin D1 expression in breast cancer cells by downregulating the JNK phosphatase DUSP3/VHR. *International journal of cancer* **121**: 39-46.

Hayes J, Peruzzi PP, Lawler S. 2014. MicroRNAs in cancer: biomarkers, functions and therapy. *Trends in molecular medicine* **20**: 460-469.

Hemmings BA, Restuccia DF. 2012. PI3K-PKB/Akt pathway. *Cold Spring Harbor perspectives in biology* **4**: a011189.

Henkens R, Delvenne P, Arafa M, Moutschen M, Zeddou M, Tautz L, Boniver J, Mustelin T, Rahmouni S. 2008. Cervix carcinoma is associated with an up-regulation and nuclear localization of the dual-specificity protein phosphatase VHR. *BMC Cancer* **8**: 147.

Hodgkinson K, Forrest LA, Vuong N, Garson K, Djordjevic B, Vanderhyden BC. 2018. GREB1 is an estrogen receptor-regulated tumour promoter that is frequently expressed in ovarian cancer. *Oncogene* **37**: 5873-5886.

Hu X, Chen P, Wu Y, Wang K, Xu Y, Chen H, Zhang L, Wu R, Webster KA, Yu H et al. 2016. MiR-211/STAT5A Signaling Modulates Migration of Mesenchymal Stem Cells to Improve its Therapeutic Efficacy. *Stem cells (Dayton, Ohio)* **34**: 1846-1858.

Huang CY, Tan TH. 2012. DUSPs, to MAP kinases and beyond. *Cell & bioscience* **2**: 24.

Imamachi N, Salam KA, Suzuki Y, Akimitsu N. 2017. A GC-rich sequence feature in the 3' UTR directs UPF1-dependent mRNA decay in mammalian cells. *Genome research* **27**: 407-418.

Imamachi N, Tani H, Mizutani R, Imamura K, Irie T, Suzuki Y, Akimitsu N. 2014. BRIC-seq: a genome-wide approach for determining RNA stability in mammalian cells. *Methods (San Diego, Calif)* **67**: 55-63.

Ishibashi T, Bottaro DP, Chan A, Miki T, Aaronson SA. 1992. Expression cloning of a human dual-specificity phosphatase. *Proc Natl Acad Sci U S A* **89**: 12170-12174.

Ji Z, Flaherty KT, Tsao H. 2012. Targeting the RAS pathway in melanoma. *Trends in molecular medicine* **18**: 27-35.

Katerinaki E, Evans GS, Lorigan PC, MacNeil S. 2003. TNF-alpha increases human melanoma cell invasion and migration in vitro: the role of proteolytic enzymes. *British journal of cancer* **89**: 1123-1129.

Kawamata T, Tomari Y. 2010. Making RISC. *Trends in biochemical sciences* **35**: 368-376.

Khabar KS. 2017. Hallmarks of cancer and AU-rich elements. *Wiley interdisciplinary reviews RNA* **8**.

Love MI, Huber W, Anders S. 2014. Moderated estimation of fold change and dispersion for RNA-seq data with DESeq2. *Genome biology* **15**: 550.

Lugowski A, Nicholson B, Rissland OS. 2018. Determining mRNA half-lives on a transcriptome-wide scale. *Methods (San Diego, Calif)* **137**: 90-98.

Margue C, Philippidou D, Reinsbach SE, Schmitt M, Behrmann I, Kreis S. 2013. New target genes of MITF-induced microRNA-211 contribute to melanoma cell invasion. *PloS one* **8**: e73473.

Mazar J, DeYoung K, Khaitan D, Meister E, Almodovar A, Goydos J, Ray A, Perera RJ. 2010. The regulation of miRNA-211 expression and its role in melanoma cell invasiveness. *PloS one* **5**: e13779.

Mazar J, Qi F, Lee B, Marchica J, Govindarajan S, Shelley J, Li JL, Ray A, Perera RJ. 2016. MicroRNA 211 Functions as a Metabolic Switch in Human Melanoma Cells. *Molecular and cellular biology* **36**: 1090-1108.

Mitra M, Lee HN, Coller HA. 2018. Determining Genome-wide Transcript Decay Rates in Proliferating and Quiescent Human Fibroblasts. *Journal of visualized experiments : JoVE*.

Narsai R, Howell KA, Millar AH, O'Toole N, Small I, Whelan J. 2007. Genome-wide analysis of mRNA decay rates and their determinants in Arabidopsis thaliana. *The Plant cell* **19**: 3418-3436.

Pawlik TM, Sondak VK. 2003. Malignant melanoma: current state of primary and adjuvant treatment. *Critical reviews in oncology/hematology* **45**: 245-264.

Peng Y, Croce CM. 2016. The role of MicroRNAs in human cancer. *Signal transduction and targeted therapy* **1**: 15004.

Perrot CY, Javelaud D, Mauviel A. 2013. Insights into the Transforming Growth Factor-beta Signaling Pathway in Cutaneous Melanoma. *Annals of dermatology* **25**: 135-144.

Rae JM, Johnson MD, Cordero KE, Scheys JO, Larios JM, Gottardis MM, Pienta KJ, Lippman ME. 2006. GREB1 is a novel androgen-regulated gene required for prostate cancer growth. *The Prostate* **66**: 886-894.

Rahmouni S, Cerignoli F, Alonso A, Tsutji T, Henkens R, Zhu C, Louis-dit-Sully C, Moutschen M, Jiang W, Mustelin T. 2006. Loss of the VHR dual-specific phosphatase causes cell-cycle arrest and senescence. *Nature cell biology* **8**: 524-531.

Rane MJ, Pan Y, Singh S, Powell DW, Wu R, Cummins T, Chen Q, McLeish KR, Klein JB. 2003. Heat shock protein 27 controls apoptosis by regulating Akt activation. *The Journal of biological chemistry* **278**: 27828-27835.

Robitaille H, Simard-Bisson C, Larouche D, Tanguay RM, Blouin R, Germain L. 2010. The small heat-shock protein Hsp27 undergoes ERK-dependent phosphorylation and redistribution to the cytoskeleton in response to dual leucine zipper-bearing kinase expression. *The Journal of investigative dermatology* **130**: 74-85.

Sahoo A, Lee B, Boniface K, Seneschal J, Sahoo SK, Seki T, Wang C, Das S, Han X, Steppie M et al. 2017. MicroRNA-211 Regulates Oxidative Phosphorylation and Energy Metabolism in Human Vitiligo. *The Journal of investigative dermatology* **137**: 1965-1974.

Sahoo A, Sahoo SK, Joshi P, Lee B, Perera RJ. 2019. MicroRNA-211 Loss Promotes Metabolic Vulnerability and BRAF Inhibitor Sensitivity in Melanoma. *The Journal of investigative dermatology* **139**: 167-176.

Siegel RL, Miller KD, Jemal A. 2018. Cancer statistics, 2018. *CA: a cancer journal for clinicians* **68**: 7-30.

Singer RH, Penman S. 1972. Stability of HeLa cell mRNA in actinomycin. *Nature* **240**: 100-102.

Song GQ, Zhao Y. 2015. MicroRNA-211, a direct negative regulator of CDC25B expression, inhibits triple-negative breast cancer cells' growth and migration. *Tumour Biol* **36**: 5001-5009.

Subramanian A, Tamayo P, Mootha VK, Mukherjee S, Ebert BL, Gillette MA, Paulovich A, Pomeroy SL, Golub TR, Lander ES et al. 2005. Gene set enrichment analysis: a knowledge-based approach for interpreting genome-wide expression profiles. *Proc Natl Acad Sci U S A* **102**: 15545-15550.

Tambe MB, Narvi E, Kallio M. 2016. Reduced levels of Dusp3/Vhr phosphatase impair normal spindle bipolarity in an Erk1/2 activity-dependent manner. *FEBS letters* **590**: 2757-2767.

Tani H, Mizutani R, Salam KA, Tano K, Ijiri K, Wakamatsu A, Isogai T, Suzuki Y, Akimitsu N. 2012. Genome-wide determination of RNA stability reveals hundreds of short-lived noncoding transcripts in mammals. *Genome research* **22**: 947-956.

Wang L, Chen Q, Chen Z, Tian D, Xu H, Cai Q, Liu B, Deng G. 2015. EFEMP2 is upregulated in gliomas and promotes glioma cell proliferation and invasion. *International journal of clinical and experimental pathology* **8**: 10385-10393.

Xia B, Yang S, Liu T, Lou G. 2015. miR-211 suppresses epithelial ovarian cancer proliferation and cell-cycle progression by targeting Cyclin D1 and CDK6. *Molecular cancer* **14**: 57.

Xu Y, Brenn T, Brown ER, Doherty V, Melton DW. 2012. Differential expression of microRNAs during melanoma progression: miR-200c, miR-205 and miR-211 are downregulated in melanoma and act as tumour suppressors. *British journal of cancer* **106**: 553-561.

Yang E, van Nimwegen E, Zavolan M, Rajewsky N, Schroeder M, Magnasco M, Darnell JE, Jr. 2003. Decay rates of human mRNAs: correlation with functional characteristics and sequence attributes. *Genome research* **13**: 1863-1872.

Yao L, Lao W, Zhang Y, Tang X, Hu X, He C, Hu X, Xu LX. 2012. Identification of EFEMP2 as a serum biomarker for the early detection of colorectal cancer with lectin affinity capture assisted secretome analysis of cultured fresh tissues. *Journal of proteome research* **11**: 3281-3294.

FIGURE LEGENDS

Figure 1. Transcriptome decay profile of the amelanotic melanoma cell line A375. A) Schematic of BRIC-seq ((Tani et al. 2012), see Methods). BrU-labeled RNA is collected at defined intervals after initial incubation to identify transcriptome-wide decay rates. B) Heatmap of normalized read counts and depicting decay profiles of all the filtered transcripts. Unsupervised hierarchical clustering represents subgroups clustered based on decay profile. C) Box plots showing the half-life distribution (in hours) of all the transcripts and transcript species as calculated from the filtered data. D) Gene ontology (GO) analysis showing top ten GO terms associated with the 5% most highly stable (top) and 5% most highly unstable (bottom) protein coding transcripts. E) Hallmark analysis showing top ten hallmarks associated with the 5% most highly stable (top) and 5% most highly unstable (bottom) protein coding transcripts.

Figure 2. MIR211 destabilizes transcriptome stability in A375 cells. A) Heatmap of normalized read counts depicting decay profiles of all the filtered transcripts for A375/211 cells. Hierarchical clustering represents subgroups clustered based on decay profiles. B) Box plots showing the half-life distribution (in hours) of all the transcripts and transcript species as calculated from the filtered data for A375/211 cells. C) Violin plot depicting half-lives of each individual transcript for different RNA species between A375 and A375/211 cells. D) Scatter plot depicting the correlation between half-life of a transcript in control A375 cells and the change in half-life upon MIR211 induction in A375/211 cells.
E) GSEA enrichment analysis for Gene ontology (GO) terms showing the top ten GO terms enriched for destabilized transcripts. F) GSEA enrichment analysis for hallmark terms showing the top ten hallmark terms enriched for destabilized transcripts.

Figure 3. Decay dynamics helps identify miR211 targets in A375 cells. A) Heatmap showing normalized read counts comparing expression of significantly (two-fold change, FDR <0.1) differentially expressed protein-coding genes between A375 and A375/211 cells. B) Venn diagram showing the overlap

between downregulated genes, destabilized genes, and *in silico* predicted gene targets. C) Heatmap plotting normalized read counts of selected MIR211 targets based on stringent criteria of overlap between destabilization, downregulation, and *in silico* prediction. D) Gene ontology (GO) analysis showing the top ten GO terms enriched for direct MIR211 targets. E) Graph comparing decay profile of *DUSP3* between A375 and A375/211 cells as calculated via BRIC-qPCR and showing that MIR211 reduces *DUSP3* transcript stability. F) qPCR validation of *DUSP3* downregulation upon MIR211 induction in A375 cells. G) *In silico* predicted MIR211 target sites in the *DUSP3* 3' UTR. H) I*n vitro* validation of MIR211-dependent *DUSP3* 3' UTR decay via a luciferase-based target cleavage assay.

Figure 4. DUSP3 downregulation reduces cell invasion and colony forming ability in A375 cells and alters MAPK/PI3K signaling. A) Western blot showing downregulation of DUSP3 protein in A375/211 cells and validating knockdown of DUSP3 upon transient DUSP3 siRNA (siDUSP3; 48 h post-transfection) transfection in A375 background compared to control siRNA (siNEG). B) DUSP3 knockdown does not affect A375 cell proliferation *in vitro* (right, compared to control siRNA, siNEG, based on four independent experiments). C) DUSP3 knockdown in A375 leads reduces cell invasion (right two panels; compared to control siRNA, siNEG). Reduced cell invasion is also seen in A375/211 compared to A375 cells (left two panels). Bar graph quantifying three independent trials. D) DUSP3 knockdown in A375 cells reduces colony formation (right two panels; compared to control siRNA, siNEG). Reduced colony formation is also seen in A375/211 compared to A375 cells (left two panels). Bar graph quantifying three independent trials. E) Human MAPK array depicting levels of various phosphorylated kinases with 8-minute exposure time. Boxed dots represent duplicate spots for identifying the indicated phosphorylated protein kinases. Bar graph representing normalized levels of selected (boxed) phosphorylated protein kinases for comparison between A375 vs. A375/211 and siNEG (control siRNA) and siDUSP3 (DUSP3 siRNA) conditions. F) Model of DUSP3 and MIR211-dependent dysregulation of MAPK and PI3K signaling. Significance level: * $p<0.05$; ** $p<0.005$; *** $p<0.005$.

Figure S1. BRIC-qPCR validation of BRIC-seq data. A) MYC and GAPDH decay rate was validated by BRIC-qPCR performed at time 0, 1, 2 and 6 h. Table shows the comparison of half-life obtained from BRIC-seq and BRIC-qPCR data for A375 and A375/211 conditions.

FIGURES

FIGURE 1

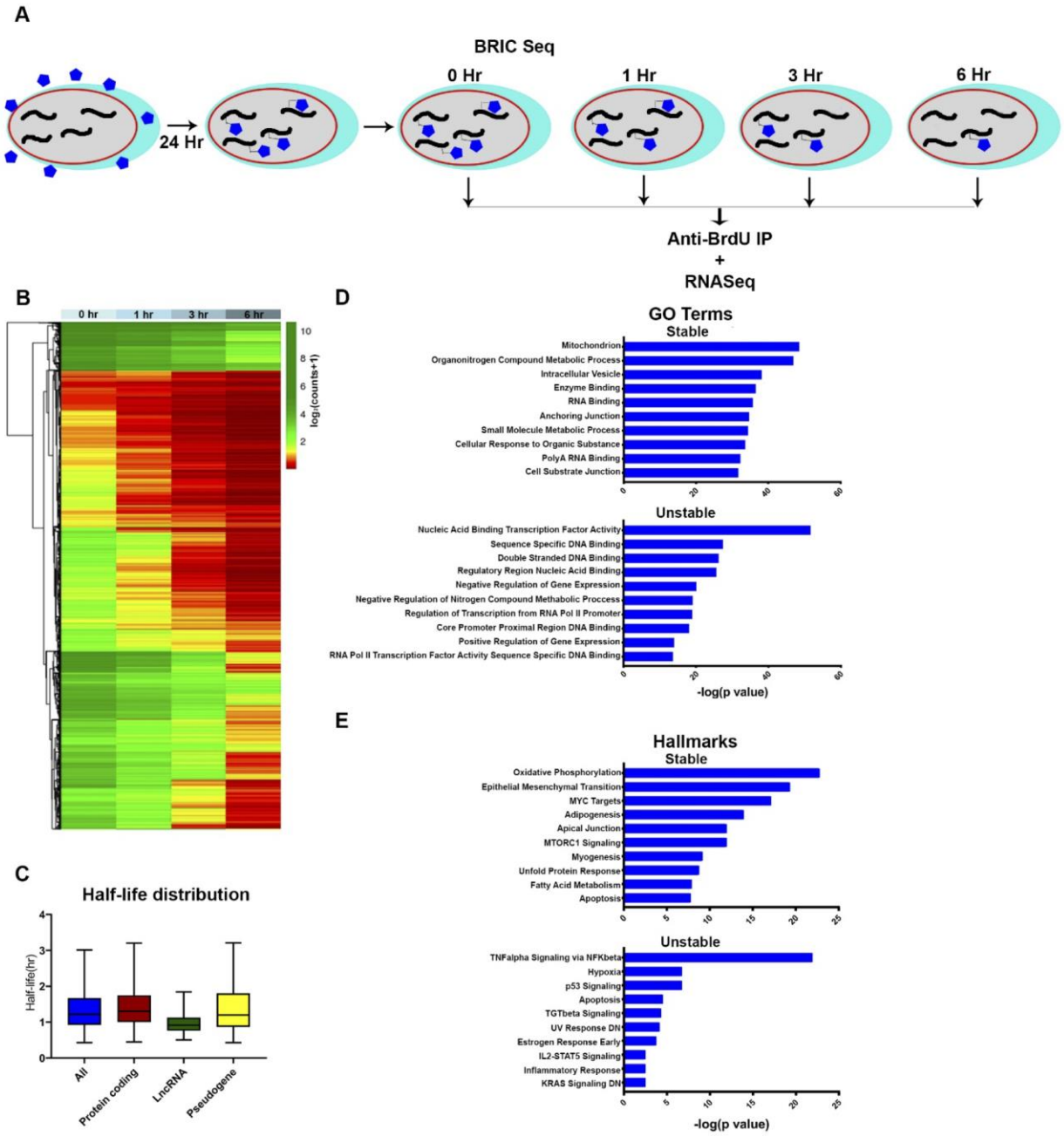

FIGURE 2

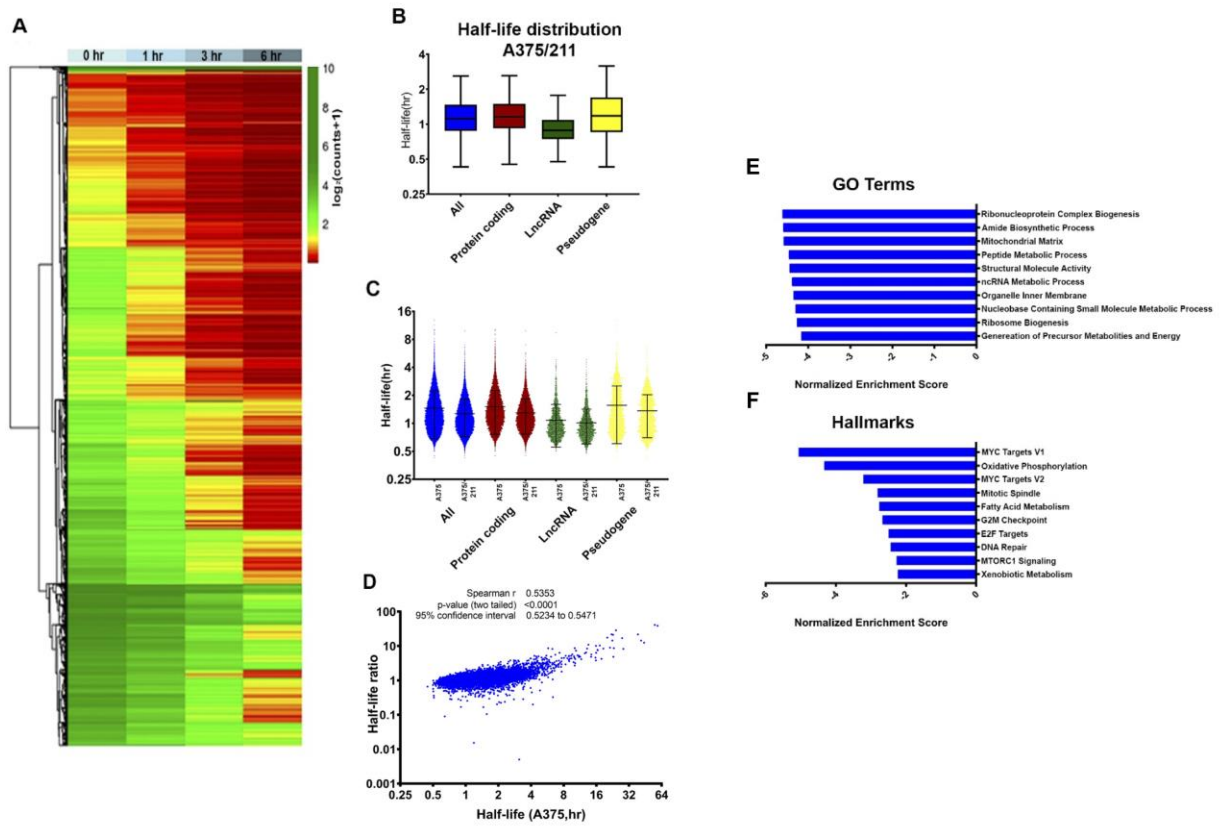
A
0 hr
1 hr
3 hr
6 hr
log2(counts+1)
B
Half-life distribution
A375/211
Half-life(hr)
All
Protein coding
LncRNA
Pseudogene
C
Half-life(hr)
All
Protein coding
LncRNA
Pseudogene
D
Spearman r 0.5353
p-value (two tailed) <0.0001
95% confidence interval 0.5234 to 0.5471
Half-life ratio
Half-life (A375,hr)
E
GO Terms
Ribonucleoprotein Complex Biogenesis
Amide Biosynthetic Process
Mitochondrial Matrix
Peptide Metabolic Process
Structural Molecule Activity
ncRNA Metabolic Process
Organelle Inner Membrane
Nucleobase Containing Small Molecule Metabolic Process
Ribosome Biogenesis
Genereation of Precursor Metabolities and Energy
Normalized Enrichment Score
F
Hallmarks
MYC Targets V1
Oxidative Phosphorylation
MYC Targets V2
Mitotic Spindle
Fatty Acid Metabolism
G2M Checkpoint
E2F Targets
DNA Repair
MTORC1 Signaling
Xenobiotic Metabolism
Normalized Enrichment Score

FIGURE 3

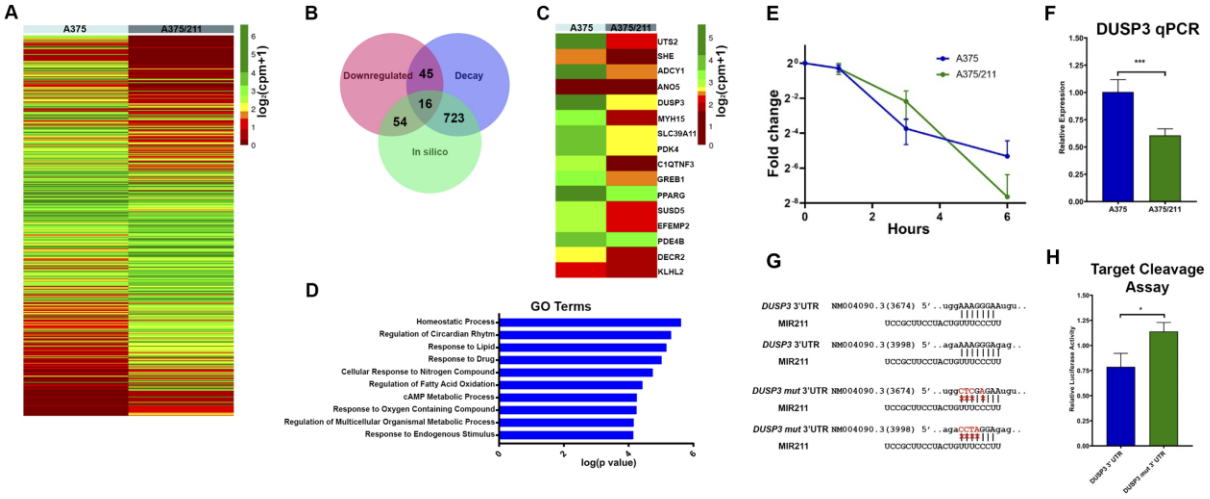
A
A375
A375/211
log(cpm+1)
B
Downregulated
45
Decay
16
54
723
In silico
C
A375
A375/211
UTS2
SHE
ADCY1
ANO5
DUSP3
MYH15
SLC39A11
PDK4
C1QTNF3
GREB1
PPARG
SUSD5
EFEMP2
PDE4B
DECR2
KLHL2
log(cpm+1)
D
GO Terms
Homeostatic Process
Regulation of Circardian Rhytm
Response to Lipid
Response to Drug
Cellular Response to Nitrogen Compound
Regulation of Fatty Acid Oxidation
cAMP Metabolic Process
Response to Oxygen Containing Compound
Regulation of Multicellular Organismal Metabolic Process
Response to Endogenous Stimulus
log(p value)
E
A375
A375/211
Fold change
Hours
F
DUSP3 qPCR
Relative Expression
A375
A375/211
G
DUSP3 3'UTR NM004090.3(3674) 5'..uggAAAGGGAAugu..
MIR211 UCCGCUUCCUACUGUUUCCCUU
DUSP3 3'UTR NM004090.3(3998) 5'..agaAAAGGGAgag..
MIR211 UCCGCUUCCUACUGUUUCCCUU
DUSP3 mut 3'UTR NM004090.3(3674) 5'..uggCCCGAGAAugu..
MIR211 UCCGCUUCCUACUGUUUCCCUU
DUSP3 mut 3'UTR NM004090.3(3998) 5'..agaCCTAGGAgag..
MIR211 UCCGCUUCCUACUGUUUCCCUU
H
Target Cleavage Assay
Relative Luciferase Activity
DUSP3 3' UTR
DUSP3 mut 3' UTR

FIGURE 4

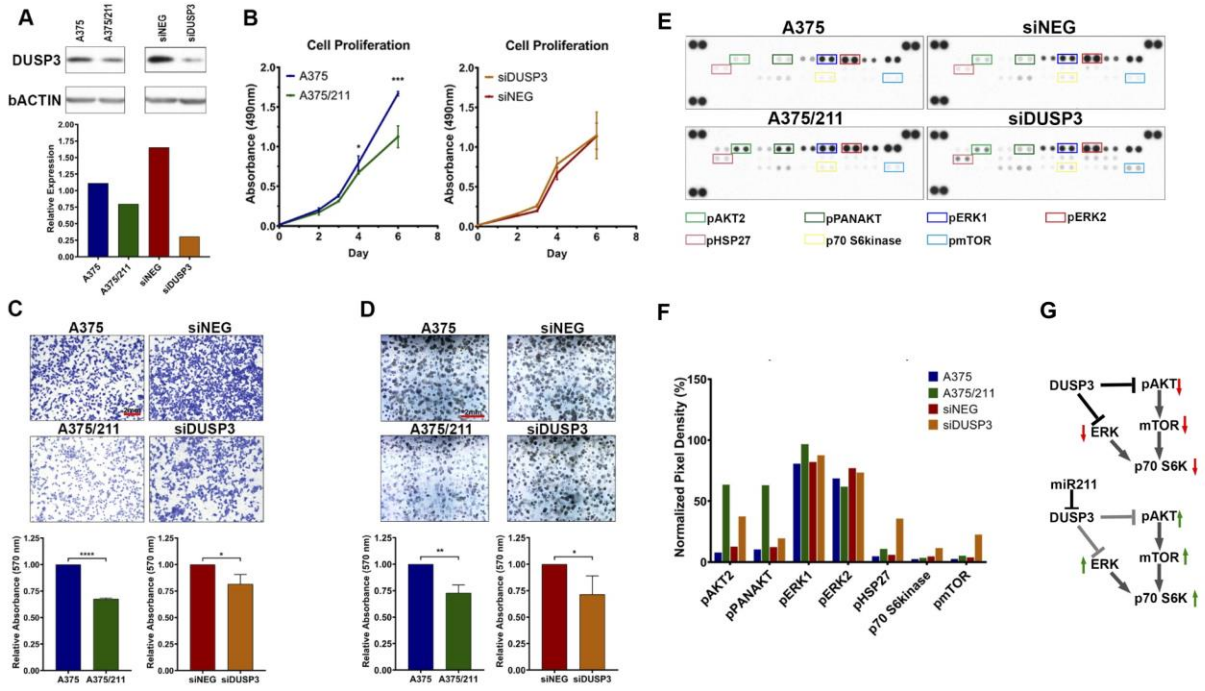
A
A375
A375/211
siNEG
siDUSP3
DUSP3
bACTIN
Relative Expression
B
Cell Proliferation
A375
A375/211
Absorbance (490nm)
Day
Cell Proliferation
siDUSP3
siNEG
Absorbance (490nm)
Day
E
A375
siNEG
A375/211
siDUSP3
pAKT2
pPANAKT
pERK1
pERK2
pHSP27
p70 S6kinase
pmTOR
C
A375
siNEG
A375/211
siDUSP3
Relative Absorbance (570 nm)
D
A375
siNEG
A375/211
siDUSP3
Relative Absorbance (570 nm)
F
A375
A375/211
siNEG
siDUSP3
Normalized Pixel Density (%)
pAKT2
pPANAKT
pERK1
pERK2
pHSP27
p70 S6kinase
pmTOR
G
DUSP3
pAKT
ERK
mTOR
p70 S6K
miR211
DUSP3
pAKT
ERK
mTOR
p70 S6K

FIGURE S1

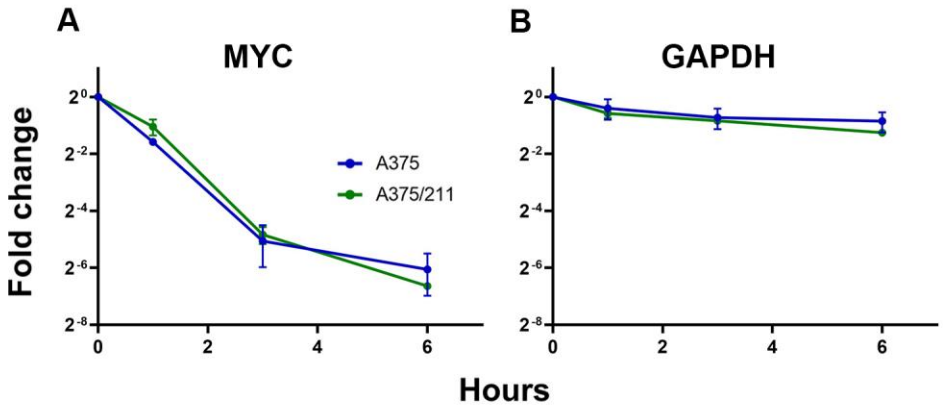

Method		MYC (half-life, h)	GAPDH (half-life, h)
BRIC-seq	A375	0.642	5.110
	A375/211	0.622	3.519
	Ratio	**1.032**	**1.452**
BRIC-qPCR	A375	0.793	5.979
	A375/211	0.765	4.011
	Ratio	**1.037**	**1.491**